

# First experimental constraint on the $^{191}\text{Os}(n, \gamma)$ reaction rate relevant to $s$ -process nucleosynthesis

I. K. B. Kullmann,<sup>1,2,\*</sup> A. C. Larsen,<sup>1</sup> T. Renstrøm,<sup>1</sup> K. S. Beckmann,<sup>1</sup> F. L. Bello Garrote,<sup>1</sup> L. Crespo Campo,<sup>1</sup> A. Görgen,<sup>1</sup> M. Guttormsen,<sup>1</sup> J. E. Midtbø,<sup>1</sup> E. Sahin,<sup>1</sup> S. Siem,<sup>1</sup> G. M. Tveten,<sup>1</sup> and F. Zeiser<sup>1</sup>

<sup>1</sup>*Department of Physics, University of Oslo, N-0316 Oslo, Norway*

<sup>2</sup>*Institut d'Astronomie et d'Astrophysique, Université Libre de Bruxelles, CP-226, 1050 Brussels, Belgium*

(Dated: September 5, 2022)

The nuclear level density and  $\gamma$ -decay strength of  $^{192}\text{Os}$  have been extracted using particle- $\gamma$  coincidence data from the  $^{192}\text{Os}(\alpha, \alpha'\gamma)^{192}\text{Os}$  reaction by means of the Oslo method. The level density is found to be a rather smooth, approximately following the constant temperature model. The  $\gamma$ -decay strength is compared to photoneutron cross-section data above the neutron separation energy, and to  $E1$  and  $M1$  strength for nuclei in this mass region derived from primary transitions following neutron capture. Our results are in good agreement with these previous data and draw a consistent picture on the  $\gamma$ -strength function in the range  $E_\gamma \approx 1.5 - 6$  MeV.

Using the measured nuclear level density and  $\gamma$ -decay strength as input to the nuclear-reaction code TALYS, we provide the first experimentally constrained Maxwellian-averaged cross section for the  $^{191}\text{Os}(n, \gamma)^{192}\text{Os}$  reaction relevant to  $s$ -process nucleosynthesis. The systematic uncertainties introduced by the normalization procedure of the level density and  $\gamma$ -strength function were investigated and propagated to the calculated Maxwellian-averaged cross section. The obtained result of the Maxwellian-averaged cross section,  $\langle \sigma \rangle_{n,\gamma} = 1134 \pm 375$  mb, is in very good agreement with the theoretical estimate provided by the KADoNiS project, giving experimental support to the adopted KADoNiS value.

## I. INTRODUCTION

Over the last century, many scientific advances have profoundly improved our understanding of the origin, current state and future of the universe. Despite this progress, our knowledge is far from complete as many salient questions remain unsolved. One of the “*Eleven Science Questions for the New Century*” [1] involves explaining the origin of the elements from iron up to uranium.

In 1957, E. Margaret Burbidge *et al.* [2] laid the very foundation of the nuclear astrophysics field in the article commonly referred to as B<sup>2</sup>FH. The famous paper proposed the hypothesis that all except the lightest chemical elements were synthesized in stars by nuclear reactions, *i.e.*, stellar nucleosynthesis. Independently, in the same year, Cameron [3] proposed a similar framework explaining the origin of the elements by several synthesis processes. Impressively, the two articles quite accurately describe the processes involved, and their theoretical framework are to a large extent still used today.

Generally speaking, the elements up to the ‘iron peak’, *i.e.*,  $Z \approx 26$ , are formed by charged-particle reactions during stellar burning. The two most dominant heavy-element nucleosynthesis processes are the slow ( $s$ -) and the rapid ( $r$ -) neutron capture process. The  $s$ -process accounts for about half of the elements heavier than iron and uses stable isotopes as stepping stones to build heavier elements. The main idea is that the neutron can easily be captured by the nucleus independent of charge, building up the heavier elements by a series of neutron captures and  $\beta$  decays [2, 3].

The  $s$ -process is known to take place in low-mass asymptotic giant branch (AGB) stars since the discovery of Tc lines by Merrill in 1952 [4]. The primary source of neu-

trons is the  $^{13}\text{C}(\alpha, n)^{16}\text{O}$  reaction taking place in  $^{13}\text{C}$  “pockets”, where  $^{13}\text{C}$  has been produced through the subsequent  $^{12}\text{C}(p, \gamma)^{13}\text{N}(\beta^+ \nu)^{13}\text{C}$  reactions [5]. However, in contrast to the robust  $r$ -process pattern found for neutron-star merger simulations (*e.g.*, Ref. [6, 7]), the  $s$ -process abundance yield depends strongly on the initial mass, the metallicity, and the mass-loss rate of the star, as well as the detailed description of the  $^{13}\text{C}$  pocket.

To test the ability of nucleosynthesis models to provide reliable  $s$ -process yields, increasingly more sophisticated nuclear reaction-network simulations are invoked (see, *e.g.*, Ref. [8]). As the  $s$ -process is following the valley of stability and has its end-point at  $^{209}\text{Bi}$ , the reaction network mainly deals with  $(n, \gamma)$  and  $\beta^-$ -decay rates. To obtain the reaction rate in a stellar environment, the cross section of interest is averaged over the Maxwell-Boltzmann velocity distribution giving the so-called Maxwellian-averaged cross section (MACS), which in turn is used to derive the reaction rate. Traditionally, MACS values relevant for the  $s$ -process are given at the neutron energy  $E_n = k_B T = 30$  keV [9].

For most of the  $(n, \gamma)$  rates of relevance for the  $s$ -process, neutron capture cross sections can be measured directly [5]. However, the so-called  $s$ -process *branch points* [10], for which the unstable compound nucleus created in the neutron capture reaction might live long enough to capture a neutron instead of undergoing  $\beta$  decay, are very difficult to measure experimentally. There are a few cases where direct measurements have been performed [5], such as for the  $^{63}\text{Ni}(n, \gamma)$  reaction [11, 12] due to the rather long half-life of  $^{63}\text{Ni}$  of about 100 years [13]. For branch-point nuclei with shorter half-lives than a few years, a direct experiment is extremely difficult to perform.

Measured  $(n, \gamma)$  cross sections for the  $s$ -process have been presented in the compilation by Bao *et al.* [14], and a thorough evaluation is available via the KADoNiS project [15]. The library includes both experimental and theoretically calculated values, and has been updated several times. For the

\* i.k.b.kullmann@fys.uio.no

$^{191}\text{Os}(n, \gamma)^{192}\text{Os}$  reaction investigated in this work, only a theoretical reaction rate is available [16], which is not surprising since  $^{191}\text{Os}$  is unstable, with a half-life of about 15 days [13]. Although this is a much shorter half-life than the important branching at  $^{185}\text{W}$  [5] with  $T_{1/2} \approx 75$  days [13], it is significantly longer than, for example, the possible branchings at  $^{186}\text{Re}$  ( $\approx 3.7$  days [13]) and  $^{148}\text{Pm}$  ( $\approx 5$  days [13]). Therefore, it is possible that  $^{191}\text{Os}$  could be an  $s$ -process branch point, and if so, it could impact the  $s$ -process yield for the heavier  $s$ -process elements.

Three nuclear input parameters are of key importance when calculating  $(n, \gamma)$  cross sections: the nuclear level density (NLD), the  $\gamma$ -strength function ( $\gamma\text{SF}$ ), and the neutron optical-model potential (n-OMP) [17]. The main goal of this work is to give a first experimental constraint on the MACS value for the  $^{191}\text{Os}(n, \gamma)^{192}\text{Os}$  reaction by means of an experimentally obtained NLD and  $\gamma\text{SF}$  of  $^{192}\text{Os}$ .

This article is organized as follows. The experimental setup and data calibration will be described in section II, while section III introduces the Oslo method utilized to extract the level density and  $\gamma$ -strength function of  $^{192}\text{Os}$ . A careful uncertainty estimate of the normalization parameters of the NLD and  $\gamma\text{SF}$  will be performed in section III C. In section IV, the experimental results will be discussed, while section V presents the Maxwellian-averaged cross section of the  $^{191}\text{Os}(n, \gamma)^{192}\text{Os}$  reaction calculated by means of the level density and  $\gamma$ -strength function of  $^{192}\text{Os}$ . A summary of the main findings and an outlook are given in Ref. section VI.

## II. EXPERIMENTAL SETUP AND DATA ANALYSIS

The experiment was performed in May 2017 at the Oslo Cyclotron Laboratory (OCL) with the goal of studying the  $^{192}\text{Os}(\alpha, \alpha'\gamma)^{192}\text{Os}$  reaction. An  $\alpha$ -beam with an energy of 30 MeV was applied with a beam current of  $\sim 4$  nA for three days. The  $^{192}\text{Os}$  target was self supported,  $> 99\%$  enriched and with a thickness of  $0.33$  mg/cm<sup>2</sup>. A self-supporting  $^{60}\text{Ni}$  target with a thickness of  $2$  mg/cm<sup>2</sup> was placed in the beam for approximately 2 hours at the beginning of the experiment for calibration purposes.

The CACTUS/SiRi detector array is designed to study particle- $\gamma$  coincidences. The SiRi detector array measures charged particles emitted in the solid angle that the array covers ( $\approx 6\%$  of  $4\pi$ ), and consists of eight separate silicon detectors in a ring placed inside the target chamber. Each silicon detector is divided into two parts, a thin  $\Delta E$  ( $130$   $\mu\text{m}$ ) and a thick  $E$  ( $1550$   $\mu\text{m}$ ) detector [18]. Each of the eight  $\Delta E$  detectors are divided into eight strips, forming a  $\Delta E$ - $E$  particle-telescope system of 64 detectors. In the current experiment, the SiRi array was placed in backward angles, covering angles from  $126^\circ$  to  $140^\circ$  between the incident trajectory and the trajectory of the emitted particle [18]. The angular resolution of the strips are  $\approx 2^\circ$  [18, 19] and the experimental resolution of the telescopes was observed to be  $\approx 235$  keV full-width half maximum for the  $^{192}\text{Os}(\alpha, \alpha'\gamma)^{192}\text{Os}$  reaction.

The energies of the coincident  $\gamma$  rays were measured by the CACTUS detector system [20] consisting of 26 collimated

NaI(Tl) scintillation detectors. Each crystal is  $5'' \times 5''$  large and was mounted on a spherical frame surrounding the target chamber giving a total measured efficiency of  $14.1(1)\%$  at  $E_\gamma = 1332.5$  keV [19, 21]. More information on the detector and data-acquisition electronics setup at OCL is given in Ref. [18, 21, 22].

The SiRi particle-telescope allows for particle identification by measuring the deposited energy of the ejected charged-particles in the thin  $\Delta E$  and thick  $E$  detector. The particles' difference in charge and mass separate them in the  $\Delta E$ - $E$  matrix. Therefore, a two dimensional gate on the emitted  $\alpha$ -particles in the  $\Delta E$ - $E$  matrix was set to select the data corresponding to the  $(\alpha, \alpha'\gamma)$  reaction. By using the known reaction kinematics, the deposited energy in the SiRi detector, *i.e.*, the  $\Delta E$ - $E$  spectra, was converted into excitation spectra  $E_x$  for the final nucleus. Then, the coincidence events were sorted into a matrix with the excitation energy,  $E_x$ , versus the  $\gamma$  energy,  $E_\gamma$ , on the  $y$ - and  $x$ -axis, and the number of counts on the  $z$ -axis. Every point in the coincidence matrix corresponds to the simultaneous detection of an  $\alpha$ -particle and  $\gamma$  ray(s) related to the  $^{192}\text{Os}(\alpha, \alpha'\gamma)^{192}\text{Os}$  reaction, see Figure 1a.

For each excitation-energy bin, the  $\gamma$  ray spectra were unfolded [23] with respect to the response of the detectors. The method developed by [23] have been proven to work well for continuum  $\gamma$  rays and preserves the experimental statistical uncertainties without introducing any artificial fluctuations. Listed in Table 1 in [19], the applied updated response functions from 2012 are shown. The resulting unfolded coincidence matrix for  $^{192}\text{Os}$  is presented in Figure 1b.

To obtain the transition probabilities a first-generation, or primary,  $\gamma$ -ray spectrum must be identified. Starting from the unfolded spectrum, the first generation spectra are obtained by an iterative subtraction method [24]. This method relies on the assumption that the decay routes of a  $\gamma$  ray from a level at an excitation-energy bin is independent of how the levels within the bin were reached. Then, the shape of the  $\gamma$ -ray spectra involving states populated by the nuclear reaction is identical to the spectra created by states populated by higher-lying energy states. Figure 1c shows the first generation matrix, or the decay probability of  $^{192}\text{Os}$  for a given excitation energy  $E_x$  and  $\gamma$ -ray energy  $E_\gamma$ . A detailed discussion of the uncertainties and errors of the unfolding and first generation method can be found in [25].

The next step in the analysis is to obtain the functional form of the NLD and the  $\gamma\text{SF}$  by means of the iteration procedure described in [26]. The  $\gamma$ -ray transmission coefficient  $\mathcal{T}$  is related to the strength function  $f$  through [27]:

$$f_{XL}(E_\gamma) = \frac{1}{2\pi} \frac{\mathcal{T}_{XL}(E_\gamma)}{E_\gamma^{(2L+1)}}. \quad (1)$$

where  $E_\gamma$  is the  $\gamma$ -ray energy with electromagnetic character  $X$  and multipolarity  $L$ . This relation is obtained by combining the expression for the  $\gamma$ -ray transmission coefficient following Blatt and Weisskopf [28],

$$\langle \Gamma_\gamma^{XL}(E_x, E_\gamma, I, \pi) \rangle = \mathcal{T}_\gamma^{XL}(E_x, E_\gamma, I, \pi) \frac{D(E_x, E_\gamma, I, \pi)}{2\pi}, \quad (2)$$

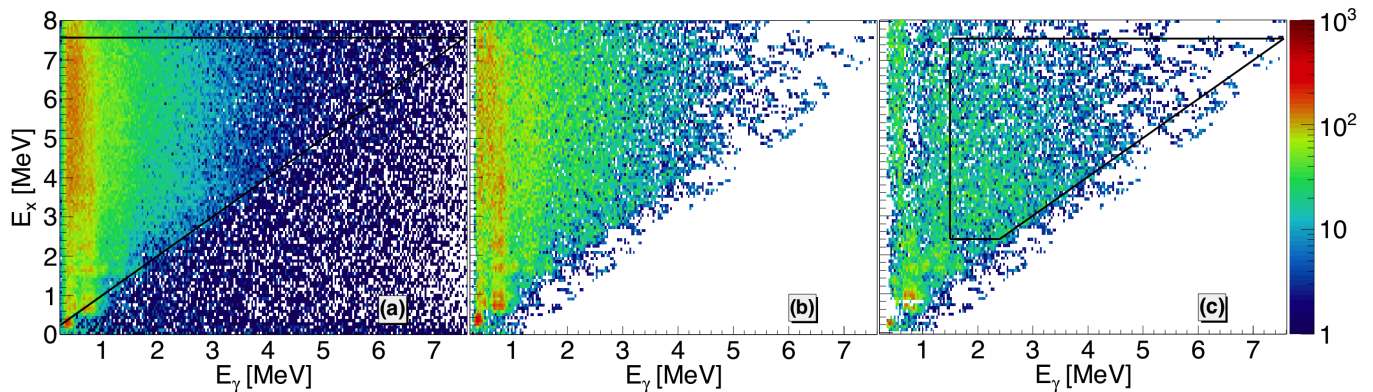


FIG. 1. (Color online) Excitation energy  $E_x$  versus  $\gamma$  energy  $E_\gamma$  for  $^{192}\text{Os}$ , (a) the original, (b) unfolded and (c) first-generation matrix. The number of counts are represented by the color scale and the bin width is 32 keV and 80keV for the x- and y-axis, respectively. Before unfolding, all data points with values larger than  $E_x = E_\gamma + \delta E_\gamma$ , where  $\delta E_\gamma$  reflects the detector resolution of the NaI(Tl), were set to zero as these counts fluctuate around zero. The black, solid lines represent the limits included in the  $\chi^2$ -minimization method.

where  $\langle \Gamma_\gamma^{XL}(E_x, E_\gamma, I, \pi) \rangle$  is the partial radiative width from excitation energy  $E_x$  and from levels with spin, parity  $I, \pi$ , and  $D$  is the average level spacing, with the definition of the  $\gamma$ SF given in Bartholomew *et al.* [29]:

$$f_{XL}(E_x, I, \pi, E_\gamma) = \frac{\langle \Gamma_\gamma^{XL}(E_x, I, \pi, E_\gamma) \rangle}{D(E_x, E_\gamma, I, \pi) E_\gamma^{2L+1}}. \quad (3)$$

By application of the Brink hypothesis [30], the dependence on  $E_x, I, \pi$  is averaged out and the  $\gamma$ -ray transmission coefficient (and correspondingly the  $\gamma$ SF) is dependent only on the  $\gamma$ -ray energy, giving Equation 1. As common practice, we assume dipole radiation ( $L = 1$ ) to be the main contribution to the experimental  $f$ , as supported by experimental data (*e.g.*, Refs. [31, 32]).

If a statistical decay process<sup>1</sup> is assumed, and by applying Fermi's golden rule [34], the experimental first-generation matrix  $P(E_x, E_\gamma)$  can be factorized into the nuclear level density  $\rho$  and the  $\gamma$ -ray transmission coefficient  $\mathcal{T}$ . In addition, the factorization assumes the Brink hypothesis [30] to be valid<sup>2</sup>, *i.e.* it is assumed that the  $\gamma$ -ray transmission coefficient is independent of excitation energy. We therefore write the factorization of the experimental first-generation matrix as [26]:

$$P(E_x, E_\gamma) = \frac{\mathcal{T}(E_\gamma) \rho(E_x - E_\gamma)}{\sum_{E_\gamma=E_\gamma^{\min}}^{E_x} \mathcal{T}(E_\gamma) \rho(E_x - E_\gamma)}, \quad (4)$$

where  $\rho(E_x - E_\gamma)$  is the level density at the final energy level after the emission of a  $\gamma$  ray of energy  $E_\gamma$  at excitation energy  $E_x$ , and  $\mathcal{T}$  is the  $\gamma$ -ray transmission coefficient. For the extraction of the level density and the transmission coefficient,

the experimental first-generation matrix is re-binned to 160 keV per bin for the  $E_x$  and  $E_\gamma$  axis. The first-generation matrix is normalized so that the sum over all  $\gamma$ -ray energies in the range  $E_\gamma^{\min} \leq E_\gamma \leq E_\gamma^{\max}$  is unity, for a given excitation energy bin  $E_x$ :

$$\sum_{E_\gamma=E_\gamma^{\min}}^{E_x} P(E_x, E_\gamma) = 1. \quad (5)$$

Here,  $E_\gamma^{\min}$  and  $E_\gamma^{\max}$  are the minimum and maximum  $\gamma$ -ray energies included in the analysis. The limits are chosen to ensure that the data employed stem from the statistical excitation energy region in the first-generation matrix  $P(E_x, E_\gamma)$ . In the present work, the upper and lower limits of the matrix was set to  $E_\gamma^{\min} = 1.5$  MeV and  $E_x^{\min} = 2.4$  MeV, while the maximum excitation energy was set to the neutron separation energy  $E_x^{\max} = 7.558$  MeV to exclude the neutron emission channel. The section of the first-generation matrix  $P$  that was included in the analysis is contained by the black solid lines in Figure 1c. Higher and lower values of  $E_x^{\min}$  do not change the results significantly the chosen  $E_\gamma^{\min}$  limit, *i.e.*, the extraction of  $\rho$  and  $\mathcal{T}$  is not sensitive to the choice of  $E_x^{\min}$  within the experimental error bars for  $^{192}\text{Os}$ .

The functional form of  $\rho$  and  $\mathcal{T}$  for  $^{192}\text{Os}$  was then uniquely determined by a  $\chi^2$  minimization [26] of Equation 4. The minimization method is only required to fulfill Equation 4, no other assumptions of the functional form of  $\rho$  and  $\mathcal{T}$  were done. The remaining task is then to normalize the NLD and the  $\gamma$ SF to experimental data.

### III. DETERMINING THE NUCLEAR LEVEL DENSITY AND THE $\gamma$ -STRENGTH FUNCTION

If one solution  $\mathcal{T}(E_\gamma)$  and  $\rho(E_f)$  of Equation 4 is known, it can be mathematically shown [26] that there exists an infinite

<sup>1</sup> The reaction leads to a compound nucleus which decays independently of how it was formed [33].

<sup>2</sup> See Refs. [25, 35] for a thorough discussion of the validity of the Brink hypothesis when applied in the Oslo method.

set of solutions given by the transformation:

$$\tilde{\rho}(E_x - E_\gamma) = A \exp[\alpha(E_x - E_\gamma)] \rho(E_x - E_\gamma), \quad (6)$$

$$\tilde{\mathcal{T}}(E_\gamma) = B \exp[\alpha E_\gamma] \mathcal{T}(E_\gamma). \quad (7)$$

Any combination of values  $A$ ,  $B$  and  $\alpha$  will yield solutions  $\tilde{\rho}$  and  $\tilde{\mathcal{T}}$  obeying:

$$P(E_x, E_\gamma) = \frac{\tilde{\mathcal{T}}(E_\gamma) \tilde{\rho}(E_x - E_\gamma)}{\sum_{E_\gamma=E_\gamma^{\min}}^{E_x} \tilde{\mathcal{T}}(E_\gamma) \tilde{\rho}(E_x - E_\gamma)}. \quad (8)$$

The solutions  $\rho$  and  $\mathcal{T}$  obtained in the  $\chi^2$ -minimization procedure are therefore the general solution of Equation 4, they contain the general shape and the functional form of the solution. The physical, or special solution is determined by the parameters  $A$ ,  $\alpha$ , and  $B$ . These parameters are acquired separately for the NLD and  $\gamma$ SF by normalizing the functions to external data.

None of the required experimental parameters for the normalization of the NLD and  $\gamma$ SF are available for  $^{192}\text{Os}$ . Therefore, these parameters have to be estimated through systematics, which introduce an additional uncertainty in the NLD and  $\gamma$ SF for  $^{192}\text{Os}$ .

#### A. Normalization of the level density

The absolute value  $A$  and the slope  $\alpha$  of the level density  $\rho$  are determined by: 1) a normalization to the number of known discrete levels at low excitation energy, and 2) the estimated level density at the neutron separation energy,  $\rho(S_n)$ .

To calculate  $\rho(S_n)$  from neutron resonance data ( $D_0$  values), the spin and parity distributions of the level density at  $S_n$  have to be known. These quantities are model dependent in this case (for some nuclei this is experimentally known), introducing a potentially large uncertainty in the normalization procedure.

In this work, only the constant-temperature (CT) formula is considered. The CT model provides a simple, analytic formula for the NLD:

$$\rho_{CT}(E) = \frac{1}{T_{CT}} \exp\left(\frac{E - E_0}{T_{CT}}\right), \quad (9)$$

where the nuclear temperature  $T_{CT}$  and the energy shift  $E_0$  serve as free parameters to be adjusted to the experimental discrete levels. The CT formula assumes an equiparity distribution, *i.e.*, that both parities contribute equally to the level density. The spin distribution is approximated by [36]:

$$g(E_x, I) \simeq \frac{2I + 1}{2\sigma_I^2(E_x)} \exp[-(I + 1/2)^2 / 2\sigma_I^2(E_x)], \quad (10)$$

for a specific excitation energy  $E_x$  and spin  $I$ . This expression is valid within the statistical model assuming random couplings of angular momenta, provided that many particles and

TABLE I. Parameters used to extract the level density within the CT model approach, in addition to the level-density parameter  $a$  and back-shift  $E_1$  for the Fermi-gas model from [38].

$a$ [MeV $^{-1}$ ]	$E_1$ [MeV]	$E_d$ [MeV]	$\sigma_d$	$T_{CT}$ [MeV]	$E_0$ [MeV]
18.472	0.328	1.1	2.8	0.5	0.331

holes are excited [36]. Following the approach of [37], the energy dependent spin cutoff parameter is introduced as:

$$\sigma_I^2(E_x) = \sigma_d^2 + \frac{E_x - E_d}{S_n - E_d} [\sigma_I^2(S_n) - \sigma_d^2], \quad (11)$$

going through two anchor points  $\sigma_d^2$  and  $\sigma_I^2(S_n)$  at the energy  $E_d$  and  $S_n$ , respectively. In this approach, the  $n$  known discrete levels at the excitation energy  $E_x = E_d = 1.1$  MeV are used to estimate an experimental spin distribution to determine the first point  $\sigma_d^2$ . Assuming a rigid moment of inertia  $\Theta = 0.0146A^{5/3}$ , the second point at  $E_x = S_n = 7.558$  MeV can be estimated through [38]:

$$\sigma_I^2(S_n) = 0.0146A^{5/3} \frac{1 + \sqrt{1 + 4aU_n}}{2a}, \quad (12)$$

where  $A$  is the mass number and  $U_n = S_n - E_1$  is the intrinsic excitation energy. The level parameter  $a$  and the energy shift parameter  $E_1$  are taken from [38]. The applied parameters to obtain the spin-cutoff parameter in this work can be found in Table I.

We can then estimate the level density at the neutron separation energy  $S_n$  from the spacing of neutron s-wave ( $\ell = 0$ ) resonances  $D_0$  following  $(n, \gamma)$  capture [26]:

$$\rho(S_n) = \frac{2\sigma_I^2}{D_0} \frac{1}{(I_t + 1) \exp[-(I_t + 1)^2 / 2\sigma_I^2] + I \exp[-I^2 / 2\sigma_I^2]}. \quad (13)$$

Here, we implement the spin cutoff parameter  $\sigma_I = \sigma_I(S_n)$  for the compound nucleus following neutron capture from Equation 11, and  $I_t$  is the ground-state spin of the target nucleus in the  $(n, \gamma)$  reaction, *i.e.*,  $9/2^-$  for  $^{191}\text{Os}$ .

In order to normalize the level density of  $^{192}\text{Os}$ , the  $D_0$  parameter of Equation 13 must be known. Unfortunately, no tabulated  $D_0$  values are available for  $^{191}\text{Os}$  for the NLD of  $^{192}\text{Os}$ . Therefore, an estimate is obtained by using available values from neutron resonance experiments of isotopes in the same mass region. In Figure 2,  $\rho(S_n)$  values for all available osmium isotopes are presented. The experimental  $D_0$  values for  $A = 187 - 193$  (except 192) are taken from [40]<sup>3</sup> (green) and [39] (black) and transformed into  $\rho(S_n)$  values by means of Equation 13. The theoretical, or systematic values (red) are

<sup>3</sup> The new, updated version of this atlas [41] (available February, 2018) was not included in this work. The impact of the few, updated  $D_0$  and  $\langle \Gamma_\gamma \rangle$  values on the recommended  $\rho(S_n)$  and  $\langle \Gamma_\gamma \rangle$  for  $^{192}\text{Os}$  was tested. The recommended values only changed by 5%, an insignificant adjustment compared to the applied uncertainties of 20 - 40%.

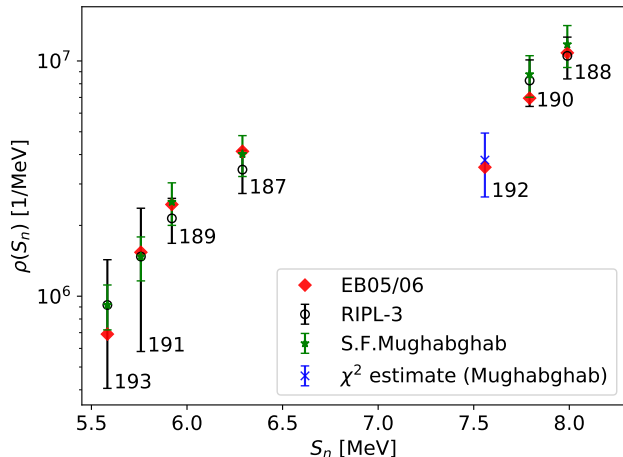


FIG. 2. (Color online) The level density at the separation energy  $\rho(S_n)$  plotted against the neutron separation energy  $S_n$ . The mass numbers  $A$  are annotated next to the data points. The values are calculated from  $D_0$  values (RIPL-3 [39], Mughabghab [40]) using spin cutoff parameters according to EB05/06 [38].

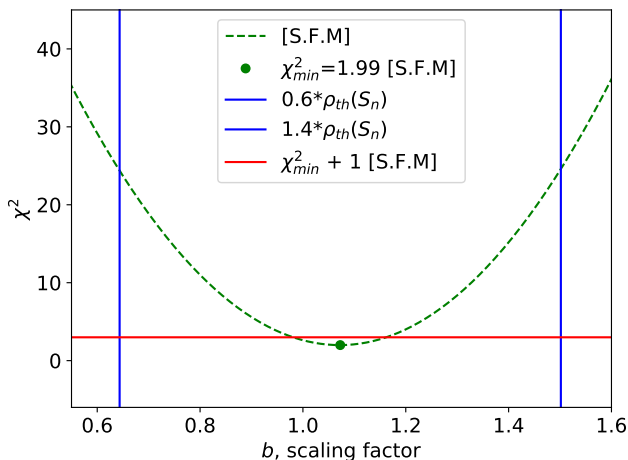


FIG. 3. (Color online) The scaling factor  $b$  versus the  $\chi^2$  value found by using experimental values from Mughabghab *et al.* (S.F.M) [40] (green), see the text. The red line represents  $\chi^2_{\min} + 1$ , and the blue lines are presenting the  $b$ -values corresponding to  $0.6\rho_{th}(S_n)$  and  $1.4\rho_{th}(S_n)$ .

provided by the phenomenological parameterization of Von Egidy and Bucurescu, hereafter named EB05/06 [38].

The EB05/06 values presented in Figure 2 are generally in good agreement with the available data in this mass region. Although the general trend for the  $D_0$  values are reproduced by the global fit of the EB05/06 parameterization, this is not a guarantee that the value for  $^{192}\text{Os}$  is well reproduced. Therefore, a  $\chi^2$ -minimization was done to estimate the level density at the neutron separation energy for  $^{192}\text{Os}$  by using the experimental values provided by [40]. The appropriate scaling factor  $b$  between the EB05/06 [38] values  $\rho_{th}(S_n)$  and the values

TABLE II. The high (H), recommended (R) and lower (L) estimates of the parameters used in the normalization procedure of the level density and the  $\gamma$ -strength function. Note that the low (high)  $D_0$  values correspond to the the high (low)  $\rho(S_n)$  values.

	$D_0$ [eV]	$\rho(S_n)$ [ $10^6 \text{ MeV}^{-1}$ ]	$\sigma_I(S_n)$	$\langle \Gamma_{\gamma 0} \rangle$ [meV]
H	5.25	4.94	7.81	107
R	3.66	3.79	7.41	79
L	2.81	2.64	6.98	61

provided by [40] was found by minimizing:

$$\chi^2 = \sum_A \frac{(b \cdot \rho_{th}(S_n) - \rho_{exp}(S_n))^2}{\Delta \rho_{exp}^2(S_n)} \quad (14)$$

where  $\Delta \rho_{exp}(S_n)$  is the listed one standard deviation uncertainty for the experimental  $D_0$  points [40] and the sum runs over  $A \in [187, 188, 189, 190, 191, 193]$ . The resulting scaling factor versus the  $\chi^2$  value is presented in Figure 3, where the minimum values at  $b = 1.073$  and  $\chi^2 = 1.99$  are highlighted. A rough error estimate, represented by the blue lines in Figure 3, of the resulting  $\rho(S_n)$  point for  $^{192}\text{Os}$  (blue in Figure 2) was done by taking the largest uncertainty of the experimental points [40] and adding a 40% relative error. Considering the spread of  $D_0$  values in the literature, 40% is a conservative estimate chosen to rather overestimate the uncertainty than underestimate it. This error analysis leads to the lower (L), recommended (R) and higher (H) estimates for the level density at the neutron separation energy listed in Table II.

Following [37], a systematic error band can be created by multiplying the rigid moment of inertia  $\Theta = 0.0146A^{5/3}$  of Equation 12 with a factor  $\eta$ . In this way, the lower (L), recommended (R) and higher (H) estimates of the spin cutoff parameter listed in Table II can be introduced by letting  $\eta \in [0.8, 0.9, 1.0]$ , respectively.

In Figure 4, the level density (black) obtained by using the recommended parameters listed in Table II is presented. The experimental data only reach up to  $\sim S_n - 1.5$  MeV, so an interpolation between the Oslo data and  $\rho(S_n)$  (blue) is done using the CT level density model (red). The slope of the experimental level density is found by forcing the level density to fit the discrete levels at  $E_x = 116$  keV and  $E_x = 1236$  keV, in addition to the CT interpolation between  $E_x = 3156$  keV and  $E_x = 6036$  keV. This procedure ensures a good reproduction of the cumulative number of levels up to  $E_x \approx 2$  MeV. The CT model parameters of Equation 9 are listed in Table I. The uncertainties presented by the black data points are statistical errors in addition to systematic errors from the unfolding and first generation method, estimated with the Oslo method software [42] as described in [26], from now on referred to as Oslo Method errors.

## B. Normalization of the $\gamma$ -strength function

The shared slope  $\alpha$  of the level density  $\rho$  and the transmission coefficient  $\mathcal{T}$  was found through the normalization of  $\rho$  in the previous subsection. The parameter  $B$ , which gives the

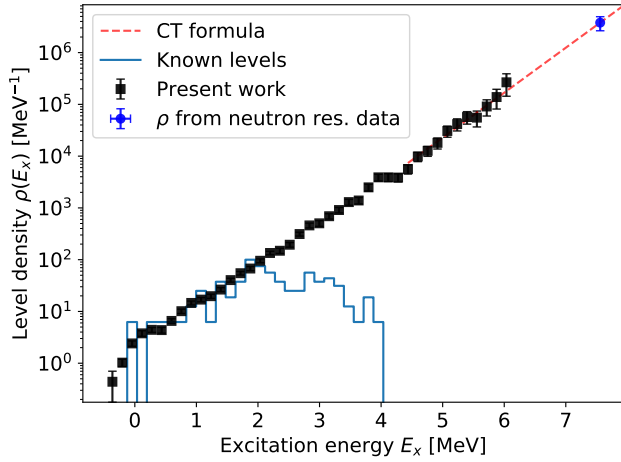


FIG. 4. (Color online) The level density versus excitation energy for the Oslo data (black). The CT interpolation between the data and  $\rho(S_n)$  (blue) is indicated by a red line in addition to the known levels (light blue).

absolute normalization of  $\mathcal{S}$ , is the only remaining unknown of Equation 7. This parameter can be constrained by the known average total radiative width,  $\langle\Gamma_{\gamma 0}\rangle$ , at  $S_n$  from  $s$ -wave neutron resonance experiments. For  $s$ -wave neutron capture on an even-even target leading to levels with spin/parity  $1/2^+$  in the compound nucleus, and using Eq. (3.1) in Ref. [27], one obtains:

$$\langle\Gamma_{\gamma 0}(S_n, I^\pi = 1/2^+)\rangle = \frac{D_0(S_n, I^\pi = 1/2^+)}{2\pi} \times \sum_{XL} \sum_{I_f} \int_0^{S_n} dE_\gamma \mathcal{T}_{XL}(E_\gamma) \rho(S_n - E_\gamma, I_f). \quad (15)$$

The summation and integration runs over all final levels with spin  $I_f$ , that are accessible by  $E1$  and  $M1$  transitions with energy  $E_\gamma$ , *i.e.*, assuming dipole radiation ( $L = 1$ ). Then, the transmission coefficient  $\mathcal{T}$  can be transformed into the  $\gamma$ -strength function  $f$  by using Equation 1.

Experimental  $\langle\Gamma_{\gamma 0}\rangle$  values are not available for  $^{192}\text{Os}$ , due to the fact that  $^{191}\text{Os}$  is unstable. Therefore, the  $\langle\Gamma_{\gamma 0}\rangle$  value at  $S_n$  was estimated through a weighted linear regression of the values presented in Figure 5, *i.e.* a simplistic first-order estimate. The average radiative widths are plotted against mass number  $A$  for available osmium isotopes in addition to the neighboring isotopes tungsten, rhenium and iridium.

An inconsistency between the  $\langle\Gamma_{\gamma 0}\rangle$  values collected from RIPL-3 [39], the n\_TOF collaboration [43] and Mughabghab [40] is revealed for the osmium isotopes in Figure 5. To investigate the discrepancy, a linear regression on the separate data sets was performed leading to a lower (L) and a higher (H) estimate of the  $\langle\Gamma_{\gamma 0}\rangle$  value for  $^{192}\text{Os}$  displayed in Table II. The lower estimate is calculated through an extrapolation using the n\_TOF values (red solid line) and the higher estimate is provided by an extrapolation using the osmium values from Mughabghab *et al.* (green dotted line).

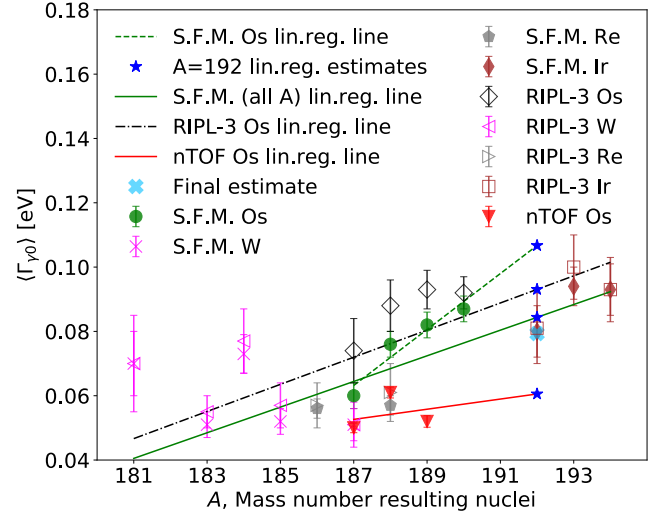


FIG. 5. (Color online) The average radiative widths  $\langle\Gamma_{\gamma 0}\rangle$  at  $S_n$  plotted against mass number  $A$  for osmium (green/black), tungsten (magenta), rhenium (gray) and iridium (brown). The data is collected from RIPL-3 [39], Mughabghab *et al.* [40] (S.F.M.) and the n\_TOF collaboration [43]. The  $\langle\Gamma_{\gamma 0}\rangle$  value for  $^{192}\text{Os}$  has been estimated through multiple weighted linear regressions, setting the weights to the inverse of the uncertainty of the points. The black dotted line is a linear regression of the RIPL-3 values, the green solid line of all the Mughabghab values, the red solid line of the n\_TOF values and the green dotted line of only the osmium points from Mughabghab.

In addition, the osmium data points display a different trend than the isotopes in the same mass region. Another estimate is therefore calculated through a linear regression of all RIPL-3  $\langle\Gamma_{\gamma 0}\rangle$  values (black solid line), and another by using all of the values provided by Mughabghab (green solid line) displayed in Figure 5. The final estimate, or the ‘recommended’ value (light blue cross) is calculated as the mean of the  $\langle\Gamma_{\gamma 0}\rangle$  values (blue points) obtained through the four approaches mentioned above.

In Figure 6, the  $\gamma$ SF obtained using the recommended  $\langle\Gamma_{\gamma 0}\rangle$  value at  $S_n$  (see Table II) is displayed together with  $(\gamma, n)$  data from [44]. The large error bars at high  $E_\gamma$  in the  $\gamma$ -strength function are directly related to the low statistics for high-energy  $\gamma$ -rays in Figure 1c. Assuming  $L = 1$  and applying the principle of detailed balance [28], the photonuclear cross section  $\sigma_{\gamma n}$ , *i.e.*, the data from [44], is transformed into the  $\gamma$ SF by [45]:

$$f(E_\gamma) = \frac{1}{3\pi^2 \hbar^2 c^2} \frac{\sigma_{\gamma n}(E_\gamma)}{E_\gamma}. \quad (16)$$

As for the level density, the uncertainties presented in Figure 6 are statistical errors and systematic errors of the unfolding and first-generation method [26], *i.e.*, Oslo method errors. An estimate of the systematic errors introduced by the normalization parameters will be performed in the next subsection.

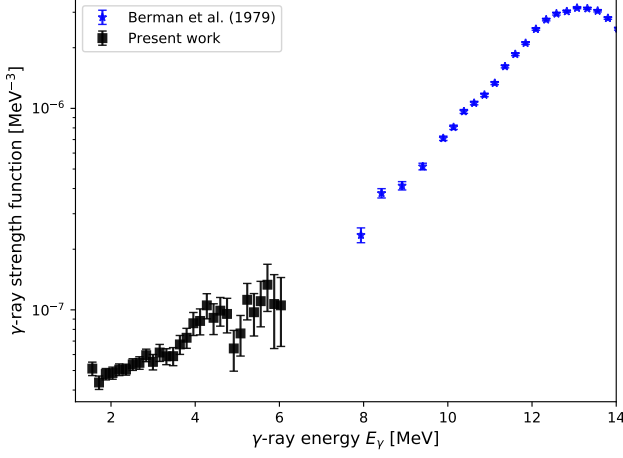


FIG. 6. (Color online) The  $\gamma$ -strength function (black) versus  $\gamma$ -ray energy obtained using the recommended  $\langle \Gamma_{\gamma 0} \rangle$  value at  $S_n$ . In addition,  $(\gamma, n)$  data (blue) from [44] is presented. Systematic errors from the normalization procedure are not included.

### C. Systematic error estimate

Often, the experimental parameters required by the normalization technique are known, and the procedure can be performed in a straightforward manner. In such cases, the uncertainty of the normalization is introduced by the model dependence of the parameter determination, and the uncertainty of the experimental values applied. As mentioned previously, no experimental normalization parameters are known for  $^{192}\text{Os}$ , introducing an additional uncertainty in the normalized solutions for the NLD and  $\gamma\text{SF}$ . Therefore, an error estimate is of utmost importance in order to quantify the significance of the results obtained.

The Oslo method software [42] propagates the statistical and systematic errors of the analysis as described in section II, but it does not take into account the systematic errors introduced by the choice of normalization parameters. Therefore, we estimate the total uncertainty in the following manner. The  $D_0$ ,  $\rho(S_n)$ ,  $\sigma_I(S_n)$  and  $\langle \Gamma_{\gamma 0} \rangle$  values in Table II were varied to obtain a systematic uncertainty band for the NLD and  $\gamma\text{SF}$ . The  $D_0$  and the  $\rho(S_n)$  values are correlated, using the lower  $D_0$  value implies using the higher  $\rho(S_n)$  value. Thus, there are only three normalization parameters to vary, *i.e.*,  $\sigma(S_n)$ ,  $\langle \Gamma_{\gamma 0} \rangle$  and  $D_0$  or  $\rho(S_n)$ .

The approximated standard deviation of the level density,  $\sigma_\rho$ , due to systematic and statistical errors was split into:

$$\sigma_{\rho,\text{high}}^2 = \rho_{\text{rec}}^2 \left[ \left( \frac{\rho_{D_0,\text{low}} - \rho_{\text{rec}}}{\rho_{\text{rec}}} \right)^2 + \left( \frac{\rho_{I,\text{high}} - \rho_{\text{rec}}}{\rho_{\text{rec}}} \right)^2 + \left( \frac{\Delta \rho_{\text{rec}}}{\rho_{\text{rec}}} \right)^2 \right], \quad (17)$$

and

$$\sigma_{\rho,\text{low}}^2 = \rho_{\text{rec}}^2 \left[ \left( \frac{\rho_{D_0,\text{high}} - \rho_{\text{rec}}}{\rho_{\text{rec}}} \right)^2 + \left( \frac{\rho_{I,\text{low}} - \rho_{\text{rec}}}{\rho_{\text{rec}}} \right)^2 + \left( \frac{\Delta \rho_{\text{rec}}}{\rho_{\text{rec}}} \right)^2 \right], \quad (18)$$

due to the asymmetric higher and lower estimates, compared to the recommended level density  $\rho_{\text{rec}}$ , listed in Table II. Here,  $\rho_{D_0,\text{low}}$  corresponds to the NLD obtained using the lower  $D_0$  value (giving a high NLD) and  $\rho_{D_0,\text{high}}$  corresponds to the NLD obtained using the higher  $D_0$  value (giving a low NLD). Furthermore,  $\rho_{I,\text{low}}$  is obtained using the low spin cutoff value  $\sigma_{I,\text{low}}$  and  $\sigma_{I,\text{high}}$  gives the  $\rho_{I,\text{high}}$  value (see also Table II). The Oslo method error of the recommended NLD is denoted as  $\Delta \rho_{\text{rec}}$ .

Similarly, for the  $\gamma$ -strength function the standard deviation due to systematic and statistical errors  $\sigma_f$  was estimated as:

$$\sigma_{f,\text{high}}^2 = f_{\text{rec}}^2 \left[ \left( \frac{f_{D_0,\text{low}} - f_{\text{rec}}}{f_{\text{rec}}} \right)^2 + \left( \frac{f_{I,\text{high}} - f_{\text{rec}}}{f_{\text{rec}}} \right)^2 + \left( \frac{f_{\langle \Gamma_{\gamma 0} \rangle,\text{high}} - f_{\text{rec}}}{f_{\text{rec}}} \right)^2 + \left( \frac{\Delta f_{\text{rec}}}{f_{\text{rec}}} \right)^2 \right], \quad (19)$$

and

$$\sigma_{f,\text{low}}^2 = f_{\text{rec}}^2 \left[ \left( \frac{f_{D_0,\text{high}} - f_{\text{rec}}}{f_{\text{rec}}} \right)^2 + \left( \frac{f_{I,\text{low}} - f_{\text{rec}}}{f_{\text{rec}}} \right)^2 + \left( \frac{f_{\langle \Gamma_{\gamma 0} \rangle,\text{low}} - f_{\text{rec}}}{f_{\text{rec}}} \right)^2 + \left( \frac{\Delta f_{\text{rec}}}{f_{\text{rec}}} \right)^2 \right]. \quad (20)$$

where  $\Delta f_{\text{rec}}$  is the Oslo method error of the recommended  $\gamma\text{SF}$ . Hence, the higher and lower values of the level density and  $\gamma\text{SF}$  within their one standard deviation limits are set to:

$$\rho_{\text{high}} = \rho_{\text{rec}} + \sigma_{\rho,\text{high}} \quad (21)$$

$$\rho_{\text{low}} = \rho_{\text{rec}} - \sigma_{\rho,\text{low}}, \quad (22)$$

and

$$f_{\text{high}} = f_{\text{rec}} + \sigma_{f,\text{high}} \quad (23)$$

$$f_{\text{low}} = f_{\text{rec}} - \sigma_{f,\text{low}}. \quad (24)$$

The resulting error band for the NLD and  $\gamma\text{SF}$  of  $^{192}\text{Os}$  are presented in Figure 7 and Figure 8, respectively.

## IV. DISCUSSION OF THE EXPERIMENTAL RESULTS

### A. The level density

In Figure 4, the nuclear level density versus excitation energy  $E_x$  for  $^{192}\text{Os}$  is displayed together with the CT formula (red) and the discrete known levels (blue). Up to  $\approx 2$  MeV, the discrete level scheme appears to be complete, *i.e.*, up to this

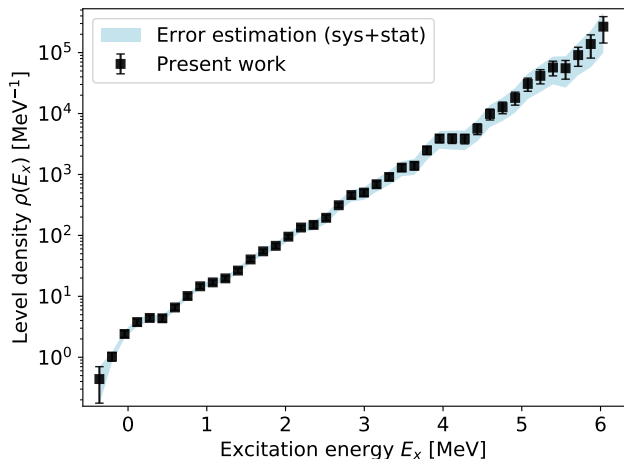


FIG. 7. (Color online) The level density versus excitation energy for the Oslo data (black). The Oslo method errors combined with the systematic error estimate of the normalization parameters are presented as the light-blue colored band.

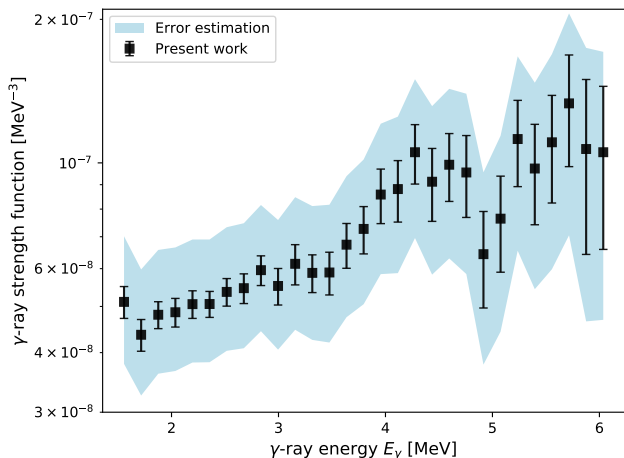


FIG. 8. (Color online) The  $\gamma$ -strength function (black) versus  $\gamma$ -ray energy for the Oslo data (black). The Oslo method errors combined with the systematic error estimate of the normalization parameters are presented as the light-blue colored band.

point the discrete levels follow the same trend as the present experimental level density. An exponential, *i.e.*, linear growth in the log scale is observed. This fits well with the CT formula, displayed in red, which has been adapted to go through the point at  $\rho(S_n)$  in addition to the experimental level density.

A quite large total uncertainty is deduced in the NLD for  $^{192}\text{Os}$  in Figure 7, in particular the last five data points have a total uncertainty larger than 50%. The Oslo method errors displayed in black have an uncertainty of  $\approx 9\%$  at minimum and  $\approx 45\%$  at the highest- $E_x$  data point. Similarly, the average of the high and low normalization uncertainty is  $\approx 12\%$  in the lowest- $E_x$  data point,  $\approx 1\%$  at minimum and  $\approx 48\%$  at the highest- $E_x$  data point. The errors calculated by the Oslo

method software, have approximately the same magnitude and a similar evolution as the uncertainty introduced by the normalization parameters.

## B. The $\gamma$ -strength function

The  $\gamma$ -strength function versus  $\gamma$ -ray energy for  $^{192}\text{Os}$  is displayed in Figure 9 together with data points from Kopecky *et al.* [31] (K.), Capote *et al.* [39] (C.), Berman *et al.* [44] (B.) and Shizuma *et al.* [46] (S.).

Similar to the NLD, the  $\gamma$ SF displays quite large uncertainties (blue band). The Oslo method errors, displayed in black in Figure 8 and 9, increase in magnitude at higher  $\gamma$ -ray energy, from  $\approx 8\%$  at the lowest- $E_\gamma$  data point, to  $\approx 40\%$  at the highest- $E_\gamma$  data point. The average of the higher and lower normalization uncertainties has a similar magnitude over the whole energy range, varying between  $\approx 31\%$  at low  $\gamma$ -ray energy, to  $\approx 46\%$  at high  $\gamma$ -ray energy. Combined, the systematic and statistical uncertainty varies between  $\approx 30\%$  at low energy, to  $\approx 60\%$  at high energy.

In general, the upper relative uncertainty estimate has a larger value than the lower relative estimate for the  $\gamma$ SF, due to the asymmetric higher and lower estimates of the  $\langle \Gamma_{\gamma 0} \rangle$  value in Table II. In addition, the smallest uncertainty of the  $\gamma$ SF is larger than the smallest error of the NLD. This is due to the  $\langle \Gamma_\gamma \rangle$  value, which only influences the uncertainty of the  $\gamma$ SF. The normalization of the NLD is not dependent on the  $\langle \Gamma_\gamma \rangle$  value, while the uncertainty of the NLD normalization parameters propagates into the  $\gamma$ SF error. Compared to the  $(\gamma, n)$  data points by Berman *et al.* [44] and Shizuma *et al.* [46], the absolute value of the  $\gamma$ SF looks reasonable.

Due to the very low statistics for  $E_\gamma > 5$  MeV and consequently large uncertainties of the present data set, it is difficult to say whether there exist any significant structures in this region of the  $\gamma$ SF. It could be that a pygmy dipole resonance (see Ref. [47] and references therein) exists in the osmium isotopes, as observed in, *e.g.*,  $^{181}\text{Ta}$  [48]. Its presence could largely affect the MACS calculations [49], but unfortunately it is not possible to conclude on the existence of such structures with the present results. Other experiments, possibly with a different probe than  $\alpha$  particles, might shed new light on this very interesting question.

## C. Separating the E1 and M1 strength

To apply the experimental  $\gamma$ SF obtained in the previous section in the cross section TALYS calculation, the contribution to the  $\gamma$ SF from the E1 and M1 strength have to be separated. The E1 and M1 strengths of the final  $\gamma$ SF were found by a fitting  $f^{\text{total}} = f_{E1}^{\text{GLO}} + f_{M1}^{\text{SLO}}$  to the Oslo data and the  $(\gamma, n)$  data points of Berman *et al.* [44] for  $^{192}\text{Os}$  in Figure 9. Here, the generalized Lorentzian (GLO) model describes the giant elec-

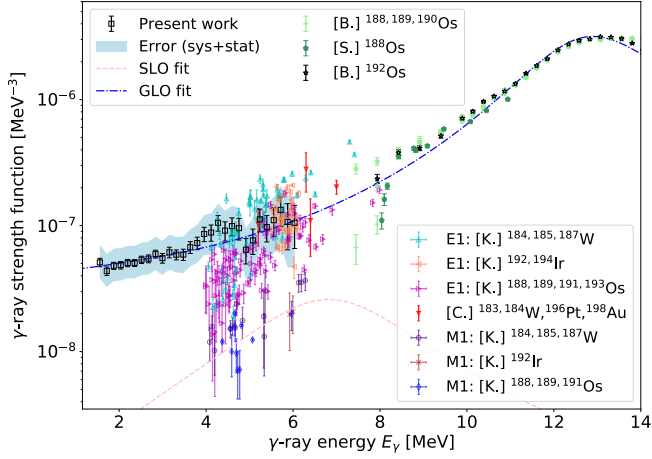


FIG. 9. (Color online) The  $\gamma$ -strength function versus  $\gamma$ -ray energy. The systematic uncertainties obtained in section III C combined with the statistical errors are presented as the colored band. In addition,  $E1$ -strength values of  $^{188,189,191,193}\text{Os}$  (magenta),  $^{192,194}\text{Ir}$  (coral) and  $^{184,185,187}\text{W}$  (cyan) and  $M2$ -strength values of  $^{188,189,191}\text{Os}$ ,  $^{192}\text{Ir}$  and  $^{184,185,187}\text{W}$  (yellow) from [31] are presented. RIPL-2  $E1$  values for  $^{183,184}\text{W}$ ,  $^{196}\text{Pt}$  and  $^{198}\text{Au}$  (red) are taken from [39]. The  $(\gamma, n)$  data is taken from Berman *et al.* [44] for  $^{188,189,190,192}\text{Os}$  and Shizuma *et al.* [46] for  $^{188}\text{Os}$ . The estimated  $E1$  and  $M1$  strengths are shown as the blue and pink dotted lines, respectively.

tric dipole resonance ( $E1$ ) as [39]:

$$f_{E1}^{\text{GLO}}(E_\gamma) = \frac{\sigma_{E1}\Gamma_{E1}}{3\pi^2\hbar^2c^2} \left( \frac{E_\gamma\Gamma_K}{(E_\gamma^2 - E_{E1}^2)^2 + E_\gamma^2\Gamma_K^2} + 0.7 \frac{\Gamma_{K,0}}{E_{E1}^3} \right), \quad (25)$$

where the last term is introduced to have a non-zero strength in the  $E_\gamma \rightarrow 0$  limit. The peak cross section, energy centroid and width parameters are denoted as  $\sigma_{E1}$ ,  $E_{E1}$  and  $\Gamma_{E1}$ , respectively. Further,  $\Gamma_K$  is a function of the  $\gamma$ -ray energy  $E_\gamma$  and the nuclear temperature parameter  $T_f$  of the final levels  $E_f = E_x - E_\gamma$  is given by:

$$\Gamma_K(E_\gamma, T_f) = \frac{\Gamma_{E1}}{E_{E1}^2} (E_\gamma^2 + 4\pi^2 T_f^2), \quad (26)$$

so that  $\Gamma_{K,0} = \Gamma_K(0, T_f)$ . The giant magnetic dipole resonance ( $M1$ ) can be described by a standard Lorentzian (SLO) curve [39]:

$$f^{\text{SLO}}(E_\gamma) = \frac{1}{3\pi^2\hbar^2c^2} \frac{\sigma_{M1}E_\gamma\Gamma_{M1}^2}{(E_\gamma^2 - E_{M1}^2)^2 + E_\gamma^2\Gamma_{M1}^2}, \quad (27)$$

where  $\sigma_{M1}$ ,  $E_{M1}$  and  $\Gamma_{M1}$  are the peak cross section, energy centroid and width of the SLO. A global parameterization [39] provides  $E_{M1} = 41 \cdot A^{-1/3}$  MeV and  $\Gamma_{M1} = 4$  MeV for a given mass number  $A$ . The peak cross section  $\sigma_{M1}$  can be determined by experimental data, or by using the relation  $f_{E1}/f_{M1} = 0.0588 \cdot A^{0.878}$  at  $\simeq 7$  MeV [39].

The number of free parameters for the SLO (Equation 27) were reduced by using the global parameterization of [39] for the SLO parameters, *i.e.*, setting the width and the energy centroid constant, the only unconstrained parameter of the SLO

function was the peak cross section  $\sigma_{\text{SLO}}$ . For the GLO parameters on the other hand, the best fit of all parameters was found by treating all parameters as free with no constraints. The optimized parameters are listed in Table III together with the corresponding uncertainty obtained by using *scipy*'s curve fitting procedure [50].

The result of the fitting procedure is presented in Figure 9 as the blue and pink dotted lines for the  $E1$  and  $M1$  strength, respectively. As expected, the overall shape of the GLO is well adjusted to the Oslo data and the giant electric dipole resonance represented by the  $(\gamma, n)$  data points. Similarly, the absolute value of the estimated  $M1$  strength agrees well with the  $^{188,189,191}\text{Os}$ ,  $^{192}\text{Ir}$  and  $^{184,185,187}\text{W}$   $M1$  values given in Ref. [31]. The listed uncertainties of the fitting procedure for the higher, recommended and lower  $\sigma_{M1}$  values are quite large compared to the uncertainties of the fitted  $E1$  parameters. The  $M1$ -component of the strength function is orders of magnitude smaller than the  $E1$  component, hence it is natural that the relative uncertainty of the fitting procedure is larger for the  $M1$  component.

A large spread in strength in the  $E1$  data provided by Kopecky *et al.* [31] of  $^{192,194}\text{Ir}$ ,  $^{188,189,191,193}\text{Os}$  and  $^{184,185,187}\text{W}$  is observed, which can be expected to be caused by Porter-Thomas-type fluctuations [51] of transition strengths. Within the statistical model with a very large number of wave-function components for each level, the Porter-Thomas distribution<sup>4</sup> of the partial  $\gamma$ -decay widths is valid, and sampling only a few transitions would lead to large fluctuations in the measured strength. It should be pointed out that none of the data points provided by [31] or [39] are  $E1$  or  $M1$  parameters of the  $^{192}\text{Os}$  isotope, and they were not included in the fit. Nevertheless, these data points do provide a consistency check, *i.e.*, that the experimental  $E1$  and  $M1$  strengths of nuclei in this mass region have approximately the same magnitude as the  $E1$  and  $M1$  components estimated for  $^{192}\text{Os}$ . Therefore, we deem that the decomposition of the experimental  $\gamma$ SF into the presented  $E1$  and  $M1$  strengths is reasonable and will be used to experimentally constrain the MACS value of the  $^{191}\text{Os}(n, \gamma)$  reaction in the next section.

## V. CALCULATION OF THE $^{191}\text{Os}(n, \gamma)$ RADIATIVE NEUTRON CAPTURE CROSS SECTION

We now use our results to constrain the MACS of the  $^{191}\text{Os}(n, \gamma)^{192}\text{Os}$  reaction by applying the experimental NLD and  $\gamma$ SF in the TALYS-1.9 [52, 53] nuclear reaction code. The recommended MACS value is calculated by applying the recommended experimental NLD and  $\gamma$ SF, in addition to a small set of input keywords. For instance, the keyword `Nlevels` was used to limit the number of known discrete levels, from tables such as [54], used by TALYS. In this case the number of levels was set to 29, as this is approximately where the discrete levels saturate, *i.e.*, where the experimental level density

<sup>4</sup> The Porter-Thomas distribution is a  $\chi^2$  distribution with 1 degree of freedom.

TABLE III. The fit parameters for the GLO and SLO functions (Equation 25 and 27), using the high (H), recommended (R) and lower (L)  $\gamma$ SF and the  $(\gamma, n)$  data points by [44]. The width  $E_{M1}$  and the energy centroid  $\Gamma_{M1}$  of the SLO function was held constant during the fitting procedure. The uncertainties were determined through the best fit procedure of [50].

	$E_{E1}$ [MeV]	$\Gamma_{E1}$ [MeV]	$\sigma_{E1}$ [mb]	$T_f$ [MeV]	$E_{M1}$ [MeV]	$\Gamma_{M1}$ [MeV]	$\sigma_{M1}$ [mb]
H	13.1(1)	2.3(2)	713(60)	1.5(2)	7.1	4	4.5(4)
R	13.2(1)	2.8(3)	615(43)	1.2(2)	7.1	4	2.1(4)
L	13.2(1)	3.0(3)	572(37)	1.0(2)	7.1	4	0.7(4)

and the discrete levels show a significantly different slope at  $E_x \approx 2$  MeV (Figure 4). In addition, a default TALYS calculation was done, *i.e.*, a calculation where all keywords used are set to default, including the level density and  $\gamma$ SF, except for the small set of keywords specified in the recommended calculation, for consistency.

To quantify the uncertainty of the experimentally constrained MACS value, the error bands of the NLD and  $\gamma$ SF are propagated into the uncertainty of the MACS values. The upper and lower limits of the NLD and  $\gamma$ SF obtained in the previous section are applied to calculate the standard deviation of the MACS value in a similar manner as to the standard deviation of the NLD and the  $\gamma$ SF in subsection section III C. We assumed all errors to be independent and added the combinations in quadrature.

The OMP applied in the recommended calculation is the default TALYS choice, the global, phenomenological potential (`localomp n`) of Koning and Delaroche [55]. Another option for the OMP in TALYS is the semi-microscopic, spherical Jeukenne-Lejeune-Mahaux (JLM) potential [56] (`jlmomp`) as adapted by Bauge *et al.* [57]. To account for the uncertainty introduced by the OMP model choice, a TALYS calculation was done with the default potential and the JLM potential. The result of this calculation was then included in the uncertainty estimate.

Another possible model choice implemented in TALYS is a width fluctuation correction factor (`widthmode`), where the default choice is the approximate expressions of Moldauer. Hilaire *et al.* [58] recommended the Moldauer expression as it better reproduced the exact expression for the width fluctuation correction factor as obtained within the Gaussian Orthogonal Ensemble approach. Therefore, we have chosen to not vary the width fluctuation input keyword in the present work.

The recommended Maxwellian-averaged cross section for the  $^{191}\text{Os}(n, \gamma)^{192}\text{Os}$  reaction calculated with the TALYS code is presented in Figure 10 together with the default TALYS run and theoretical values provided by KADoNiS [16]. The propagated uncertainty lies between  $\approx 20\%$  and  $\approx 90\%$  at low and high incident neutron energy, respectively. Although the uncertainties estimated in the current work are asymmetrical, the upper and lower standard deviations are rather similar in magnitude, providing a mean of  $\delta_{\text{mean}}^{\text{MACS}} = (348.8 \text{ mb} + 401.4 \text{ mb})/2 \approx 375 \text{ mb}$  at the energy of 30 keV, see Table IV.

For the energy range between  $E_n = k_B T = 5 - 100$  keV in Figure 10, the values provided by KADoNiS [16] agree well with the present, constrained MACS values. Interestingly, the theoretical estimate provided by the TALYS default input parameters gives a significantly smaller cross section value than

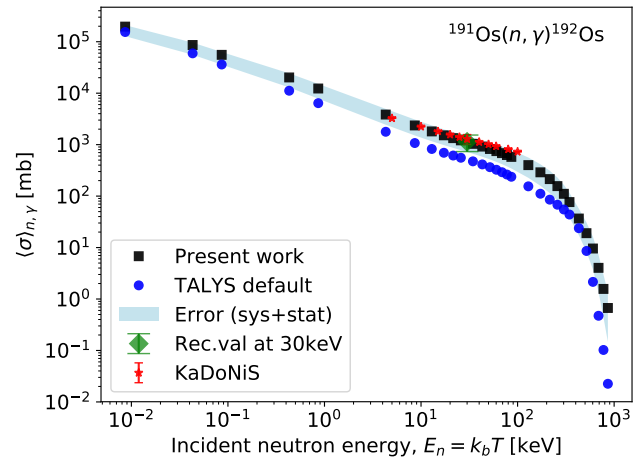


FIG. 10. (Color online) The Maxwellian-averaged  $(n, \gamma)$  cross section versus incident neutron energy  $E_n = kT$  at the stellar temperature  $T$ . The systematic and statistical uncertainties (blue band) of the recommended MACS for the  $^{191}\text{Os}(n, \gamma)^{192}\text{Os}$  reaction are presented as the colored band. In addition, values from the KADoNiS library [16] and a TALYS calculation done with default input are shown. Points at the s-process temperature  $kT = 30$  keV are highlighted with a separate marker.

the present result and the KADoNiS values over the whole energy range. This is likely due to an overall lower default level density and  $\gamma$ SF in the TALYS code compared to the present experimental data and to the models used in KADoNiS.

A comparison of the MACS values at the s-process temperature of 30 keV is presented in Table IV. As noticed before, the TALYS default value is significantly lower than the present result and the KADoNiS MACS, and lies outside of the error band. In addition, four theoretical MACS values from [59] (RaT99), [60] (HWF76), [61] (Gor02) and [62] (Gor05), listed at the KADoNiS web page [16], are presented. The deviations between the four theoretical values are large, but they all lie within the uncertainty of the present work, except for the value at 1565 mb from [61].

The magnitude of the systematic and statistical errors leads to a rather large relative error in the present result of  $\approx 33\%$  in contrast to  $\approx 22\%$  for the theoretical KADoNiS cross sections. Nevertheless, it is rewarding to observe that the theoretical value provided by KADoNiS is consistent and well within the uncertainty of the experimentally constrained MACS obtained in this work.

TABLE IV. The Maxwellian-averaged ( $n, \gamma$ ) cross sections with corresponding standard deviation  $\delta_{\text{MACS}}$  (in the unit of mb) at the  $s$ -process temperature  $k_B T = 30$  keV for the  $^{191}\text{Os}(n, \gamma)^{192}\text{Os}$  reaction. Values from KADoNiS [16] (KAD), the TALYS [63] default run (DEF) and the present work (OCL18) are compared. Four other theoretical MACS values, as cited in [16], from [59] (RaT99), [60] (HWF76), [61] (Gor02) and [62] (Gor05) calculated in 2000, 1976, 2002 and 2005, respectively, are listed.

	OCL18	KAD	DEF	RaT99	HWF76	Gor02	Gor05
$\langle \sigma \rangle_{n,\gamma}$	1134	1290	523	802	1090	1565	1399
$\delta_{\text{MACS}}$	375	280	-	-	-	-	-

## VI. SUMMARY AND OUTLOOK

In this work, we have obtained the first experimentally constrained Maxwellian-averaged cross section for the  $^{191}\text{Os}(n, \gamma)^{192}\text{Os}$  reaction relevant to the  $s$ -process nucleosynthesis. The nuclear level density and the  $\gamma$ -strength function of  $^{192}\text{Os}$  have been extracted from  $\alpha - \gamma$  coincidence data using the Oslo method and normalized by means of parameters estimated from neutron-resonance data of isotopes in the vicinity of  $^{192}\text{Os}$ . An estimation of the uncertainties introduced by the normalization parameters was done, and the resulting error band was propagated into the calculated MACS values.

No significant structures are revealed in the nuclear level density of  $^{192}\text{Os}$  and the exponential growth of the constant temperature model describes the level density well. The uncertainties of the  $\gamma$ SF are slightly larger than the errors of the level density ( $\approx 30 - 60\%$ ), but the overall absolute value agrees well with ( $\gamma, n$ ) data and  $E1$  and  $M1$  strengths provided by external data. The poor statistics at  $E_\gamma > 5$  MeV and the

correspondingly large uncertainties in the  $\gamma$ SF in this region makes it difficult to conclude whether a pygmy dipole resonance is present or not. More information from experiments with different probes would be highly desirable to address this issue.

The experimentally constrained result of the Maxwellian-averaged cross section,  $\langle \sigma \rangle_{n,\gamma} = 1134 \pm 375$  mb at 30 keV, is consistent with the theoretical predictions listed in the KADoNiS library. The TALYS default calculation, on the other hand, yields a  $\approx 50\%$  lower Maxwellian-averaged cross section value compared to the present result, lying outside of the experimental error bar.

In the future, to study the role of the  $^{191}\text{Os}(n, \gamma)^{192}\text{Os}$  reaction as a possible  $s$ -process branch point, it would be interesting to implement the current result in an  $s$ -process nucleosynthesis reaction network including all branch points in this mass region.

The extracted NLD and  $\gamma$ SF data, as well as the calculated cross section are available in the Supplemental Material.

## ACKNOWLEDGMENTS

This work was financed through ERC-STG-2014 under grant agreement no. 637686. A. C. L. acknowledges support from the ChETEC COST Action (CA16117), supported by COST (European Cooperation in Science and Technology) and A. G. acknowledge support from the Norwegian Research Council grant no. 263030. The authors would like to thank J. C. Müller, P. A. Sobas, and J. C. Wikne at the Oslo Cyclotron Laboratory for operating the cyclotron and providing excellent experimental conditions.

- 
- [1] N. R. Council, *Connecting Quarks with the Cosmos: Eleven Science Questions for the New Century* (The National Academies Press, Washington, DC, 2003).
- [2] E. M. Burbidge, G. R. Burbidge, W. A. Fowler, and F. Hoyle, *Review of Modern Physics* **29** (1957), <https://doi.org/10.1103/RevModPhys.29.547>.
- [3] A. G. W. Cameron, *Publications of the Astronomical Society of the Pacific* **69**, 201 (1957).
- [4] P. W. Merrill, *The Astrophysical Journal* **116**, 21 (1952).
- [5] F. Käppeler, R. Gallino, S. Bisterzo, and W. Aoki, *Reviews of Modern Physics* **83**, 157 (2011).
- [6] S. Goriely, J.-L. Sida, J.-F. Lemaître, S. Panebianco, N. Dubray, S. Hilaire, A. Bauswein, and H.-T. Janka, *Phys. Rev. Lett* **111**, 242502 (2013).
- [7] O. Just, A. Bauswein, R. Ardevol Pulpillo, S. Goriely, and H.-T. Janka, *Monthly Notices of the Royal Astronomical Society* **448**, 541 (2015).
- [8] C. Cescutti, R. Hirschi, N. Nishimura, J. W. den Hartogh, T. Rauscher, A. S. J. Murphy, and S. Cristallo, *Monthly Notices of the Royal Astronomical Society* **478**, 4101 (2018).
- [9] W. Ratynski and F. Käppeler, *Phys. Rev. C* **37**, 595 (1988).
- [10] R. A. Ward, M. J. Newman, and D. D. Clayton, *Astrophysical Journal Supplement* **31**, 33 (1976).
- [11] C. Lederer *et al.*, *Phys. Rev. Lett* **110**, 022501 (2013).
- [12] M. Weigand *et al.*, *Phys. Rev. C* **92**, 045810 (2015).
- [13] Data extracted using the NNDC On-Line Data Service from the NUDAT 2.7 database. URL <http://www.nndc.bnl.gov/nudat2/>...
- [14] Z. Bao, H. Beer, F. Käppeler, F. Voss, K. Wisshak, and T. Rauscher, *Atomic Data and Nuclear Data Tables* **76**, 70 (2000).
- [15] I. Dillmann, M. Heil, F. Käppeler, R. Plag, T. Rauscher, and F. Thielemann, *AIP Conference Proceedings* **819**, 123 (2006), <https://aip.scitation.org/doi/pdf/10.1063/1.2187846>.
- [16] Data extracted using the KADoNiS On-Line Data Service. URL <http://www.kadonis.org>. Accessed: 2018-05-01..
- [17] M. Arnould, S. Goriely, and K. Takahashi, *Physics Reports* **450**, 97 (2007), [arXiv:0705.4512](https://arxiv.org/abs/0705.4512).
- [18] M. Guttormsen, A. Bürger, T. E. Hansen, and N. Lietaer, *Nuclear Instruments and Methods in Physics Research, Section A: Accelerators, Spectrometers, Detectors and Associated Equipment* **648**, 168 (2011).
- [19] L. Crespo Campo, F. L. Bello Garrote, T. K. Eriksen, A. Gørgen, M. Guttormsen, K. Hadynska-Klek, M. Klintejord, A. C. Larsen, T. Renstrøm, E. Sahin, S. Siem, A. Springer, T. G. Tornyi, and G. M. Tveten, *Physical Review C* **94**, 044321 (2016).

- [20] M. Guttormsen, A. Atac, G. Løvholden, S. Messelt, T. Ramsøy, J. Rekstad, T. F. Thorsteinsen, T. S. Tveter, and Z. Zelazny, *Phys. Scr.* **T 32**, 54 (1990).
- [21] M. Guttormsen, A. Atac, G. Lsvhsiden, S. Messelt, T. Ramssy, J. Rekstad, T. F. Thorsteinsen, and T. S. Tveter, (1990).
- [22] A.-C. Larsen, *Statistical properties in the quasi-continuum of atomic nuclei*, Ph.D. thesis (2008).
- [23] M. Guttormsen, T. S. Tveter, L. Bergholt, F. Ingebretsen, and J. Rekstad, *Nuclear Instruments and Methods in Physics Research A* **374**, 371 (1996).
- [24] M. Guttormsen, T. Ramsøy, and J. Rekstad, *Nuclear Instruments and Methods in Physics Research* **255**, 518 (1987).
- [25] A. C. Larsen, M. Guttormsen, M. Kr̃tička, E. Běták, A. Bürger, A. Görgen, H. T. Nyhus, J. Rekstad, A. Schiller, S. Siem, H. K. Toft, G. M. Tveten, A. V. Voinov, and K. Wikan, *Physical Review C - Nuclear Physics* **83** (2011), 10.1103/PhysRevC.83.034315.
- [26] A. Schiller, L. Bergholt, M. Guttormsen, E. Melby, J. Rekstad, and S. Siem, *Nuclear Instruments and Methods in Physics Research, Section A: Accelerators, Spectrometers, Detectors and Associated Equipment* **447**, 498 (2000), arXiv:9910009 [nucl-ex].
- [27] J. Kopecky and M. Uhl, *Phys. Rev. C* **41**, 1941 (1990).
- [28] J. M. Blatt and V. F. Weisskopf, *Theoretical Nuclear Physics* (John Wiley & Sons, Inc., 1952) pp. 389 (transmission coefficient), 530 (detailed balance).
- [29] G. A. Bartholomew, E. D. Earle, A. J. Ferguson, J. W. Knowles, and M. A. Lone, *Gamma-Ray Strength Functions* (Springer Science + Business Media, 1973) p. 229324.
- [30] D. M. Brink, ., Ph.D. thesis, Oxford University (1955).
- [31] J. Kopecky, S. Goriely, S. Péru, S. Hilaire, and M. Martini, *Physical Review C* **95**, 054317 (2017).
- [32] A. C. Larsen *et al.*, *Phys. Rev. Lett.* **111**, 242504 (2013).
- [33] N. Bohr, *Nature* **137**, 344 (1936).
- [34] M. Guttormsen, A. C. Larsen, A. Bürger, A. Görgen, S. Harisopoulos, M. Kmiecik, T. Konstantinopoulos, M. Kr̃tička, A. Lagoyannis, T. Lönnroth, K. Mazurek, M. Norrby, H. T. Nyhus, G. Perdikakis, A. Schiller, S. Siem, A. Spyrou, N. U. Syed, H. K. Toft, G. M. Tveten, and A. Voinov, *Physical Review C - Nuclear Physics* **83**, 1 (2011), arXiv:arXiv:1009.3409v2.
- [35] M. Guttormsen, A. C. Larsen, A. Görgen, T. Renstrøm, S. Siem, T. G. Tornyi, and G. M. Tveten, *Phys. Rev. Lett.* **116**, 012502 (2016).
- [36] T. Ericson, *Advances in Physics* **9**, 425 (1960), <https://doi.org/10.1080/00018736000101239>.
- [37] M. Guttormsen, S. Goriely, A. C. Larsen, A. Görgen, T. W. Hagen, T. Renstrøm, S. Siem, N. U. Syed, G. Tagliente, H. K. Toft, H. Utsunomiya, A. V. Voinov, and K. Wikan, *Physical Review C* **96**, 1 (2017).
- [38] T. von Egidy and D. Bucurescu, *Physical Review C - Nuclear Physics* **72** (2005), 10.1103/PhysRevC.72.044311.
- [39] R. Capote, M. Herman, P. Obložinský, P. G. Young, S. Goriely, T. Belgya, A. V. Ignatyuk, A. J. Koning, S. Hilaire, V. A. Plujko, M. Avrigeanu, O. Bersillon, M. B. Chadwick, T. Fukahori, Z. Ge, Y. Han, S. Kailas, J. Kopecky, V. M. Maslov, G. Reffo, M. Sin, E. S. Soukhovitskii, and P. Talou, *Nuclear Data Sheets* **110**, 3107 (2009).
- [40] S. F. Mughabghab, *Atlas of Neutron Resonances*, 5th ed. (Elsevier, Amsterdam, 2006).
- [41] S. F. Mughabghab, *Atlas of Neutron Resonances*, sixth ed. (Elsevier, Amsterdam, 2018).
- [42] Oslo Method Software. doi: <https://doi.org/10.5281/zenodo.1153994>.,.
- [43] K. Fujii, M. Mosconi, A. Mengoni, C. Domingo-Pardo, F. Käppeler, U. Abbondanno, G. Aerts, H. Álvarez-Pol, F. Alvarez-Velarde, S. Andriamonje, J. Andrzejewski, P. Assimakopoulos, L. Audouin, G. Badurek, P. Baumann, F. Bečvá, F. Belloni, E. Berthoumieux, S. Bisterzo, M. Calviani, F. Calviño, D. Cano-Ott, R. Capote, A. Carrillo De Albornoz, P. Cennini, V. Chepel, E. Chiaveri, N. Colonna, G. Cortes, A. Couture, J. Cox, M. Dahlfors, S. David, I. Dillmann, R. Dolfini, W. Dridi, I. Duran, C. Eleftheriadis, M. Embid-Segura, L. Ferrant, A. Ferrari, R. Ferreira-Marques, L. Fitzpatrick, H. Fraiss-Koelbl, W. Furman, R. Gallino, I. Goncalves, E. Gonzalez-Romero, A. Goverdovski, F. Gramegna, E. Griesmayer, C. Guerrero, F. Gunsing, B. Haas, R. Haight, M. Heil, A. Herrera-Martinez, M. Igashira, S. Isaev, E. Jericha, Y. Kadi, D. Karamanis, D. Karadimos, M. Kerveno, V. Ketlerov, P. Koehler, V. Kononov, E. Kossionides, M. Kr̃tička, C. Lamboudis, H. Leeb, A. Lindote, I. Lopes, M. Lozano, S. Lukic, J. Marganec, L. Marques, S. Marrone, C. Massimi, P. Mastinu, P. M. Milazzo, C. Moreau, F. Neves, H. Oberhammer, M. Oshima, S. O'Brien, J. Pancin, C. Papachristodoulou, C. Papadopoulos, C. Paradela, N. Patronis, A. Pavlik, P. Pavlopoulos, L. Perrot, R. Plag, A. Plompen, A. Plukis, A. Poch, J. Praena, C. Pretel, J. Quesada, T. Rauscher, R. Reifarth, M. Rosetti, C. Rubbia, G. Rudolf, P. Rullhusen, J. Salgado, L. Sarchiapone, I. Savvidis, C. Stephan, G. Tagliente, J. L. Tain, L. Tassan-Got, L. Tavora, R. Terlizzi, G. Vannini, P. Vaz, A. Ventura, D. Villamarin, M. C. Vincente, V. Vlachoudis, R. Vlastou, F. Voss, S. Walter, H. Wendler, M. Wiescher, and K. Wisshak, *Physical Review C - Nuclear Physics* **82**, 1 (2010).
- [44] B. L. Berman, D. D. Faul, R. A. Alvarez, P. Meyer, and D. L. Olson, *Physical Review, Part C, Nuclear Physics* **19**, 1205 (1979).
- [45] P. Axel, *Proceedings of the International Symposium on Nuclear Structure* (IAEA Vienna, 1968) p. 299.
- [46] T. Shizuma, H. Utsunomiya, P. Mohr, T. Hayakawa, S. Goko, A. Makinaga, H. Akimune, T. Yamagata, M. Ohta, H. Ohgaki, Y. W. Lui, H. Toyokawa, A. Uritani, and S. Goriely, *Physical Review C - Nuclear Physics* **72**, 1 (2005).
- [47] D. Savran, T. Aumann, and A. Zilges, *Progress in Particle and Nuclear Physics* **70**, 210 (2013).
- [48] A. Makinaga *et al.*, *Phys. Rev. C* **90**, 044301 (2014).
- [49] N. Tsoneva, S. Goriely, H. Lenske, and R. Schwengner, *Phys. Rev. C* **91**, 044318 (2015).
- [50] Non-linear least squares method, SciPy org. URL [https://docs.scipy.org/doc/scipy/reference/generated/scipy.optimize.curve\\_fit.html](https://docs.scipy.org/doc/scipy/reference/generated/scipy.optimize.curve_fit.html)..
- [51] C. E. Porter and R. G. Thomas, *Phys. Rev* **104**, 483 (1956).
- [52] A. J. Koning, S. Hilaire, and M. Duijvestijn, *Nuclear Data for Science and Technology* (EDP Sciences; eds O. Bersillon *et al.*, 2008) p. 211.
- [53] A. J. Koning and D. Rochman, *Nuclear Data Sheets* **113**, 2841 (2012).
- [54] Data extracted using the NNDC On-Line Data Service from the ENSDF database. URL <https://www.nndc.bnl.gov/ensdf/>. Accessed: 2017-2018.,.
- [55] A. J. Koning and J. P. Delaroche, *Nucl. Phys. A* **713**, 231 (2003).
- [56] J.-P. Jeukenne, A. Lejeune, and C. Mahaux, *Phys. Rev. C* **16**, 80 (1977).
- [57] E. Bauge, J. P. Delaroche, and M. Girod, *Phys. Rev. C* **63**, 024607 (2001).
- [58] S. Hilaire, C. Lagrange, and A. J. Koning, *Annals of Physics* **306**, 209 (2003).

- [59] T. Rauscher and F. K. Thielemann, *Atomic Data Nucl. Data Tables* **75**, 1 (2000).
- [60] J. Holmes, S. Woosley, W. Fowler, and B. Zimmerman, *Atomic Data Nucl. Data Tables* **18**, 305 (1976).
- [61] S. Goriely, “Hauser-feshbach rates for neutron capture reactions.” (2002), Version: 2002, URL <http://www-astro.ulb.ac.be/Html/hfr.html>.
- [62] S. Goriely, “Hauser-feshbach rates for neutron capture reactions.” (2005), Version: 8/29/2005, URL <http://www-astro.ulb.ac.be/Html/hfr.html>.
- [63] S. Goriely, S. Hilaire, and A. J. Koning, *Astronomy & Astrophysics* **487**, 767 (2008), [arXiv:0806.2239](https://arxiv.org/abs/0806.2239).